Available online at www.sciencedirect.com

SciVerse ScienceDirect

Magnetic Resonance Imaging 30 (2012) 230–246

MAGNETIC RESONANCE IMAGING

Multispectral MR images segmentation based on fuzzy knowledge and modified seeded region growing

Geng-Cheng Lin[a], Wen-June Wang[a,*], Chung-Chia Kang[b], Chuin-Mu Wang[c]

[a]*Department of Electrical Engineering, National Central University, Jhongli City, Taiwan 320, R.O.C.*
[b]*Identification and Security Technology Center, Industrial Technology Research Institute, Chutung, Taiwan 310, R.O.C.*
[c]*Department of Computer Science and Information Engineering, National Chinyi University of Technology, Taiping, Taiwan 411, R.O.C.*

Received 23 December 2010; revised 15 August 2011; accepted 18 September 2011

Abstract

Magnetic resonance imaging (MRI) is a valuable diagnostic tool in medical science due to its capability for soft-tissue characterization and three-dimensional visualization. One potential application of MRI in clinical practice is brain parenchyma classification and segmentation. Based on fuzzy knowledge and modified seeded region growing, this work proposes a novel image segmentation method, called Fuzzy Knowledge-Based Seeded Region Growing (FKSRG), for multispectral MR images. In this work, fuzzy knowledge includes the fuzzy edge, fuzzy similarity and fuzzy distance, which are obtained from relationships between pixels in multispectral MR images and are applied to the modified seeded regions growing process. In conventional regions merging, the final number of regions is unknown. Therefore, a Target Generation Process is proposed and applied to support conventional regions merging, such that the FKSRG method does not over- or undersegment images. Finally, two image sets, namely, computer-generated phantom images and real MR images, are used in experiments to assess the effectiveness of the proposed FKSRG method. Experimental results demonstrate that the FKSRG method segments multispectral MR images much more effectively than the Functional MRI of the Brain Automated Segmentation Tool, K-means and Support Vector Machine methods.

Keywords: Magnetic resonance imaging (MRI); Multispectral; Segmentation; Classification; Seeded region growing (SRG)

1. Introduction

Magnetic resonance imaging (MRI) is a very effective diagnostic approach, as it has an unparalleled capability for soft-tissue characterization and three-dimensional (3D) visualization. Notably, MRI produces a sequence of multiple spectral images using three MR parameters, namely, spin–lattice (T1), spin–spin, (T2) and dual echo–echo proton density (PD). A sequence of images for a specific anatomical area can be generated by appropriately choosing echo time (TE), repetition time (TR) and the three MR parameters. Furthermore, the spectral correlation among the image sequence produces information that spatial correlation cannot provide. Thus, MRI is a more helpful image modality than X-ray Computer Tomography for analyzing soft tissues and organs [1,2]. A potential application of MRI in clinical practice is brain tissue classification or segmentation for normal and pathological tissues (e.g., tumors). Notably, MRI is the first step in dealing with a wide range of clinical problems. Tissue abnormalities, such as heterotopia, lissencephaly, brain atrophy and cerebral infarction, can be identified from the volume, shape and regional distribution of brain tissue.

Many computer-assisted methods for analyzing MR images, such as orthogonal subspace projection (OSP) [3,4], filter-based methods [5,6], neural networks [7–10], fuzzy C-means (FCM) [11–15] and knowledge-based techniques [16], have been reported over the last 15 years [3–20]. For instance, OSP is a mixed pixel classification method that models an image pixel as a linear mixture of various material substances in image data [3,4]. Signature abundance can be estimated and updated recursively using a Kalman filter, and the abruptly changing signature abundance is detectable using an abundance state equation [6].

* Corresponding author.
E-mail address: wjwang@ee.ncu.edu.tw (W.-J. Wang).

0730-725X/$ – see front matter.
doi:10.1016/j.mri.2011.09.008

Moreover, neural networks perform well in segmenting brain tissues and have been compared to classical maximum likelihood methods [7–10]. A knowledge-based system as a multispectral tool can effectively segment tumors without human supervision [16]. Zhang et al. [17] developed a new brain tissues segmentation framework that integrates the hidden Markov random field (MRF) model, associated MRF-Maximum a posteriori (MAP) estimation and expectation–maximization fitting procedures. Recently, multimodal brain MRI segmentation based on hidden Markov chains, an artificial immune system approach and adaptive FCM was proposed in Refs. [18–20]. The principal aim of this work is to classify and segment normal and pathological tissues, gray matter (GM), white matter (WM), cerebral spinal fluid (CSF) and tumors from multispectral MR images of the brain.

Seeded region growing (SRG), a hybrid method [21], starts by assigning seeds and grows regions by merging pixels into their most similar neighboring seeded region. Seeded region growing is robust for a large variety of images because local information, such as region similarity, boundaries and smoothness, are considered. However, the selection of initial seeds markedly influences segmentation results. How to assign initial seeds is a major issue in SRG. The authors in Refs. [22,23] assigned pixels between edge regions as initial seeds. The similarity in a local region is also utilized to select initial seeds automatically [24]. To avoid initial seeds appearing in detailed and complex background (BKG), the authors in Ref. [25] applied color quantization to an image in advance and then used a smoothness measurement, the J value, to choose initial seeds.

Multispectral images have the advantage of providing rich spectral information and correlations via different bands. These benefits cannot be obtained from a single (one-band) image. In medical images, objects of interest are generally soft tissues that are deformable and cannot be analyzed by shape. The shapes of soft tissues in images are represented by spatial information and spatial correlations. This work proposes a novel SRG-based image segmentation method for multispectral MR images called Fuzzy Knowledge-Based Seeded Region Growing (FKSRG). Fuzzy knowledge (fuzzy edge, fuzzy image pixel similarity and fuzzy distance) is obtained from pixel spectral and spatial information in multispectral images. Therefore, the proposed method performs segmentation without relying on object shapes only, and fuzzy edge and fuzzy image pixel similarity are used to select initial seeds automatically. The proposed fuzzy edge detection method is a modified version of that developed by Kang and Wang [26]. Fuzzy distance is utilized to determine the difference between a pixel and region in consequent regions growing. The conventional region growing method, which is modified to ensure that a pixel on an edge is processed later than other pixels, is applied to multispectral MR images. In conventional regions merging, the final number of regions is unknown. To guarantee that the proposed method does not over- or undersegment images, a proposed Target Generation Process (TGP) is applied for regions merging. The TGP is an unsupervised approach that generates a set of potential targets iteratively. Fuzzy sets and fuzzy reasoning play major roles in the TGP. Several experiments using MR images are performed to assess the effectiveness of the FKSRG method in tissue classification and segmentation. The proposed FKSRG method is compared with the K-means method, the Functional MRI of the Brain Automated Segmentation Tool (FAST) method [17,27] and the Support Vector Machine (SVM) [28] to further evaluate its performance.

The remainder of this paper is organized as follows. Section 2 introduces an overview of the proposed method and multispectral MR images. Section 3 describes the fuzzy edge and fuzzy similarity detection approach. Section 4 introduces the modified SRG procedure and TGP. Section 5 uses a set of experiments to evaluate the performance of FKSRG in MRI classification and segmentation. Section 6 gives conclusions.

2. Overview of proposed method and multispectral MR images

2.1. Overview of the proposed method

The proposed FKSRG method has several subprocesses — fuzzy edge determination, fuzzy similarity computation, initial seeds selection, modified regions growing, regions merging and the proposed TGP. Fig. 1 shows a flowchart of the proposed FKSRG method. Fuzzy edge and fuzzy image pixel similarity, which are obtained from spectral and spatial information in multispectral MR images, are subsequently used to select automatically initial seeds. In the resulting modified regions growing method, fuzzy distance is used to determine the difference between a pixel and a region. Finally, the TGP supports conventional regions merging to ensure that the proposed method does not over- or undersegment images. Detailed descriptions of proposed method are presented in Sections 3 and 4.

2.2. Multispectral MR images

We suppose a multispectral MR image contains C bands (channels), each of which is $L\times N$ in size. In multispectral image processing, the information of a multispectral image is viewed as a 3D space, and let $\mathbf{r}=[r_1, r_2,\ldots, r_C]^T$ represent a pixel vector, in which r_1, r_2 and r_C are the intensity of the first, second and C-th band pixel, respectively. Notably, the pixel vector located at position (x,y) in an image is denoted as $\mathbf{r}_{x,y}=[r_1(x,y), r_2(x,y),\ldots, r_C(x,y)]^T$. Therefore, a multispectral MR image can be viewed as a cuboid, where the third dimension is a spectral dimension specified by the TR/TE parameters. Each image pixel is actually a column vector, in which each component corresponds to a specific TR/TE parameter value. Further, the size of a multispectral MR

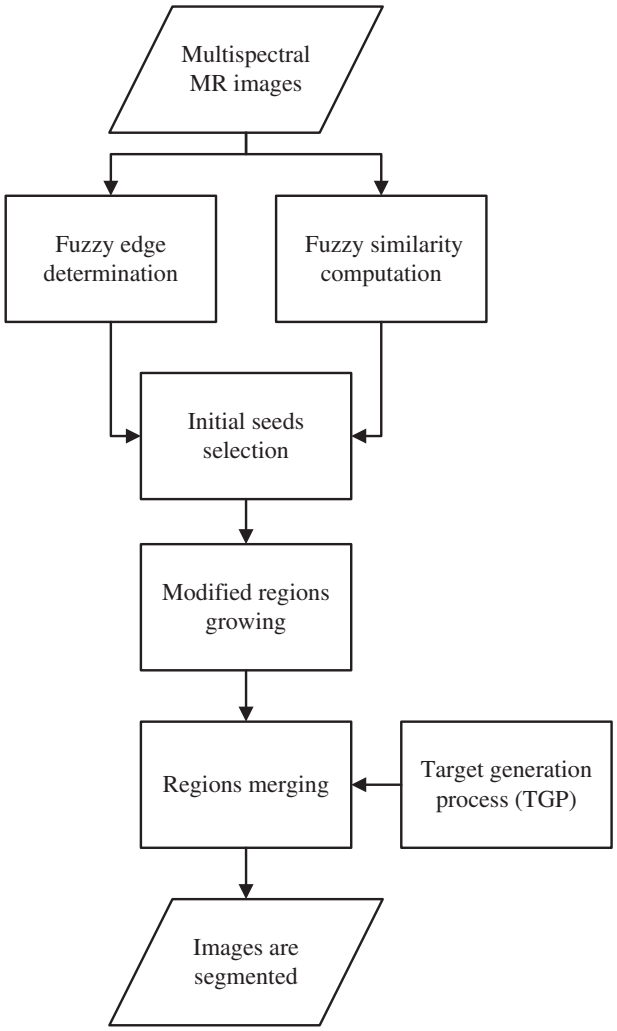

Fig. 1. Flowchart of the FKSRG.

image is $L \times N \times C$. To simplify this representation, all equations in this work are presented in vector form.

3. Fuzzy edge determination and fuzzy similarity computation

3.1. Fuzzy edge determination

In this subsection, the fuzzy edges are determined by spectral and spatial information in multispectral images. First, consider a 3×3 sliding window, whose center is the current pixel (vector) $\mathbf{x}_{x,y}$; the pixels in the sliding window are represented as $\mathbf{x}_n$, n=1, 2,..., 9 (Fig. 2). An edge usually occurs in one of four possible patterns (Fig. 3). In the edge pattern of direction 1, nine pixels can be divided into two sets, S_0^1 and S_1^1, where $S_0^1=\{\mathbf{x}_1, \mathbf{x}_2, \mathbf{x}_3, \mathbf{x}_4, \mathbf{x}_5, \mathbf{x}_7, \mathbf{x}_8\}$ and $S_1^1=\{\mathbf{x}_3, \mathbf{x}_6, \mathbf{x}_9\}$. Similarly, $S_0^2=\{\mathbf{x}_1, \mathbf{x}_2, \mathbf{x}_3, \mathbf{x}_4, \mathbf{x}_5, \mathbf{x}_6\}$ and $S_1^2=\{\mathbf{x}_7, \mathbf{x}_8, \mathbf{x}_9\}$ are for the edge in direction 2, $S_0^3=\{\mathbf{x}_1, \mathbf{x}_2, \mathbf{x}_3, \mathbf{x}_5, \mathbf{x}_6, \mathbf{x}_9\}$ and $S_1^3=\{\mathbf{x}_4, \mathbf{x}_7, \mathbf{x}_8\}$ are for the edge of direction 3, and $S_0^4=\{\mathbf{x}_1, \mathbf{x}_2, \mathbf{x}_3, \mathbf{x}_4, \mathbf{x}_5, \mathbf{x}_7\}$ and $S_1^4=\{\mathbf{x}_6, \mathbf{x}_8, \mathbf{x}_9\}$ are for the edge in direction 4. Then, the fuzzy edge distance, Edge

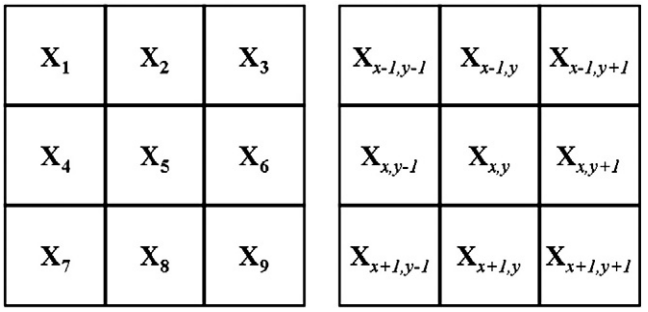

Fig. 2. The 3×3 sliding window with the center $\mathbf{x}_{x,y}$ and its neighboring pixels; the pixels in the sliding window are represented as $\mathbf{x}_n$, n=1, 2,..., 9.

(c), c=1, 2, 3, 4, is defined between S_0^c and S_1^c for direction c and c=1, 2, 3, 4, respectively, as in Eq. (1).

$$\mathrm{Edge}(c) = \min\left(\frac{||\mathbf{m}_0 - \mathbf{m}_1||}{w}, 1\right), \tag{1}$$

where $\mathbf{m}_0$ and $\mathbf{m}_1$ are the vector means of pixels in S_0^c and S_1^c, respectively, and w is set to 30. w=30 was obtained by our experimental experiences. We suggest to set w in the region [20, 150]. If w is set as a smaller value, the detailed (weak) edges would be enhanced, and the similar objects would be segmented effectively. But if the w is set too small, the algorithm would cost more time in region growing. For the center pixel, $\mathbf{x}_{x,y}$, let the maximal edge intensity $E_{x,y}$ in Eq. (2) be the fuzzy membership degree of

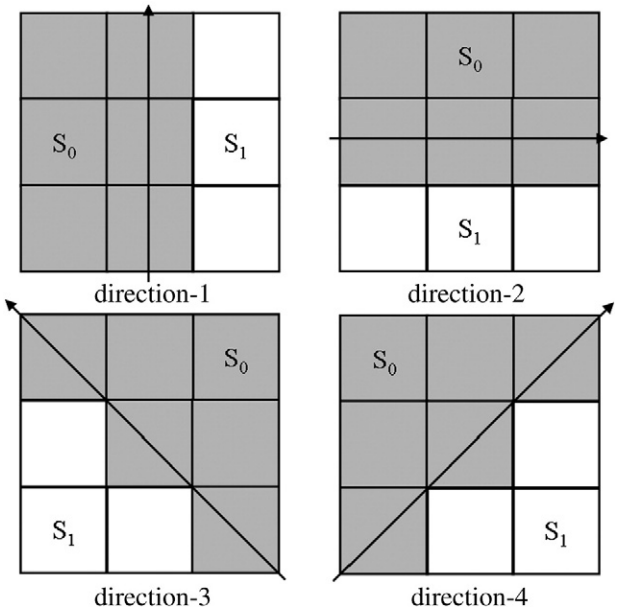

Fig. 3. Four possible edge patterns of different directions. In each edge pattern direction, nine pixels of the 3×3 sliding window are divided into two sets, S_0 and S_1.

"the current pixel is an edge," and the corresponding edge direction, $D_{x,y}$, is represented in Eq. (3).

$$E_{x,y} = \max_{c\in\{1,\ 2,\ 3,\ 4\}}(\mathrm{Edge}(c)), \tag{2}$$

$$D_{x,y} = \mathrm{Arg}\left(\max_{c\in\{1,\ 2,\ 3,\ 4\}}(\mathrm{Edge}(c))\right). \tag{3}$$

After all pixels in the image are processed via the above procedures, the edge map $\mathbf{E}=[E_{x,y}]$, x=2, 3,…, $L-1$; y=2, 3,…, $N-1$, and direction map $\mathbf{D}=[D_{x,y}]$, x=2, 3,…, $L-1$; y=2, 3,…, $N-1$, of the entire image are generated. Therefore, all pixels were assigned fuzzy membership degree of "the current pixel is an edge" and one edge direction of four patterns. Some pixels may be assigned seemingly wrong edge directions, but the corresponding fuzzy membership degrees of "the current pixel is an edge" are not large. In order to ensure that the real edges are found correctly, the neighboring fuzzy membership degrees of "the current pixel is an edge" must be considered. The fuzzy membership degree $DE_{x,y}$ of "the current pixel is a connected edge" for each pixel is defined as follows:

$$\text{If } D_{x,y}=1,\ \text{then } DE_{x,y}=\frac{1}{3}\left(E_{x-1,y}+E_{x,y}+E_{x+1,y}\right). \tag{4a}$$

$$\text{If } D_{x,y}=2,\ \text{then } DE_{x,y}=\frac{1}{3}\left(E_{x,y-1}+E_{x,y}+E_{x,y+1}\right). \tag{4b}$$

$$\text{If } D_{x,y}=3,\ \text{then } DE_{x,y}=\frac{1}{3}\left(E_{x-1,y-1}+E_{x,y}+E_{x+1,y+1}\right). \tag{4c}$$

$$\text{If } D_{x,y}=4,\ \text{then } DE_{x,y}=\frac{1}{3}\left(E_{x+1,y-1}+E_{x,y}+E_{x-1,y+1}\right). \tag{4d}$$

Conversely, the fuzzy membership degree of "the current pixel is not a connected edge," $NDE_{x,y}$, is defined as:

$$NDE_{x,y}=1-DE_{x,y}. \tag{5}$$

Both fuzzy membership degrees, $DE_{x,y}$ and $NDE_{x,y}$, for each pixel are recorded for selection of initial seeds in Section 4.1.

3.2. Fuzzy similarity computation

In Section 3.1, the $DE_{x,y}$ and $NDE_{x,y}$ for each pixel are determined. Then, Eq. (6) determines fuzzy similarity $S_{x,y}$ between each current pixel $\mathbf{x}_{x,y}$ and its corresponding neighbors.

$$S_{x,y}=1-\frac{1}{9}\sum_{n=1}^{9}\min\left(\frac{||\mathbf{x}_n-\mathbf{x}_{\mathrm{mean}}||}{w},1\right), \tag{6}$$

where $\mathbf{x}_n$, n=1, 2,…, 9 and $\mathbf{x}_{mean}$ are nine pixels in the sliding window whose center is $\mathbf{x}_{x,y}$ and their mean of vectors, respectively. Here, fuzzy similarity $S_{x,y}$ of each pixel is also recorded and used to select initial seeds in subsection 4.1.

4. Modified SRG

The conventional SRG method has three major steps — seeds selection, regions growing and regions merging. To select initial seeds appropriately, fuzzy edge and fuzzy similarity are used to select initial seeds. Thus, the conventional SRG needs one more step of preprocessing. Therefore, SRG in this work is called the modified SRG method.

4.1. Initial seeds selection and postprocessing

The initial seed pixel should have a high similarity to its neighbors [24] and not be on an edge or in a detailed region [23]. Therefore, the criterion for initial seeds selection is

$$\text{If } \min\left(NDE_{x,y},S_{x,y}\right)\geq T,\ \text{then } \mathbf{x}_{x,y} \text{ is a seed}, \tag{7}$$

where T is a threshold.

Each connected component of seed pixels is taken as one seed. Hence, the generated seed can be one pixel or one region with several connected seeds. A label number is assigned to each seeded region, and each region's mean pixel vector $\mathbf{R}_z$, z=1, 2,…, Z is recorded, where Z is the number of seeded regions. The neighbors of all seed regions are then recorded in a sorted list M, which is the set of unlabeled pixels. Significantly, in the conventional SRG step, the pixel in M with minimal distance will be firstly assigned to one of neighboring regions. In the proposed method, the minimal fuzzy distance d is defined in Eq. (8):

$$d=\min_{z=1,2,\ldots J}\left(\frac{||\mathbf{x}^M_{x,y}-\mathbf{R}_z||}{w},1\right). \tag{8}$$

where the $\mathbf{x}^M{}_{x,y}$ means the pixel $\mathbf{x}_{x,y}$ in the list M and d is defined as the minimal fuzzy distance between the pixel $\mathbf{x}^M{}_{x,y}$ and the mean pixel vectors of J neighboring seeded regions. And then let the d_M be a measurement which denotes the relation between fuzzy distance and the fuzzy degree of connected edge. The d_M is composed of d and $DE_{x,y}$, shown in Eq. (9):

$$d_M=d\cdot DE_{x,y}. \tag{9}$$

The pixels on edge or near edge are classified difficultly. Because some pixels near them are not assigned to any seed regions. In the proposed method, if a pixel in M is on an edge, its corresponding d_M is generally larger than the pixels not on an edge because of $DE_{x,y}$ in Eq. (8). Therefore, this ensures that the pixel on an edge is processed later than other pixels in M for the region growing step. In conventional regions growing and the proposed method, the processing pixel is assigned to one neighboring region. The modified region growing process is now introduced in the next subsection.

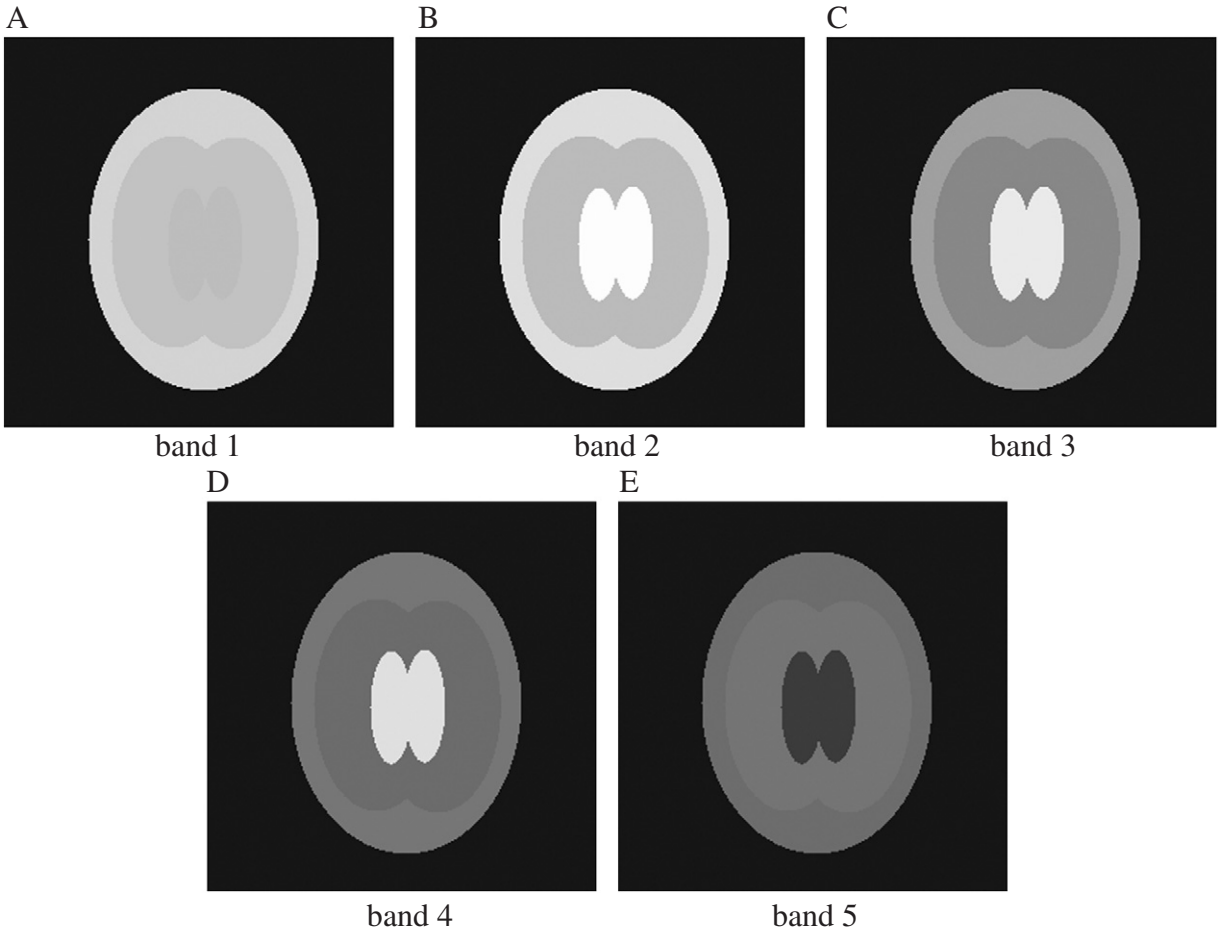

Fig. 4. Five bands of an ellipse image used for simulations, where band 1 is the PD-weighted simulated image; bands 2, 3 and 4 are T2-weighted simulated images; and band 5 is the T1-weighted simulated image.

4.2. Modified regions growing

In this step, seeded regions grow pixel by pixel. First, check the first pixel in M, i.e., the pixel in M with the smallest d_M. In conventional SRG, three cases exist for neighbors of this pixel.

- First, if only one neighbor is labeled, then the pixel is labeled as the same region as the labeled neighbor.
- Second, if more than one neighbor is labeled and the labels are the same, then the pixel is labeled as the same region as labeled neighbors.
- Third, if more than one neighbor is labeled and the labels differ, then the pixel is labeled in the region that has the smallest d to the pixel.

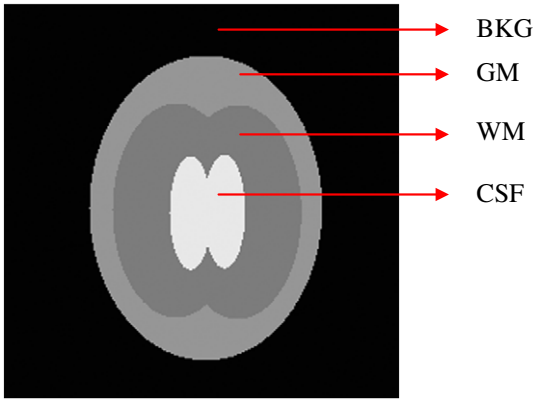

Fig. 5. The structure areas of three simulated cerebral tissues corresponding to GM, WM and CSF in the ellipse image. From the periphery to the center are BKG, GM, WM and CSF.

Table 1
Intensities used for the five bands of ellipse image in Fig. 4

	MRI parameter	GM	WM	CSF	BKG
Band 1	TR/TE=2500 ms/25 ms	207	188	182	3
Band 2	TR/TE=2500 ms/50 ms	219	180	253	3
Band 3	TR/TE=2500 ms/75 ms	150	124	232	3
Band 4	TR/TE=2500 ms/100 ms	105	94	220	3
Band 5	TR/TE=500 ms/11.9 ms	95	103	42	3

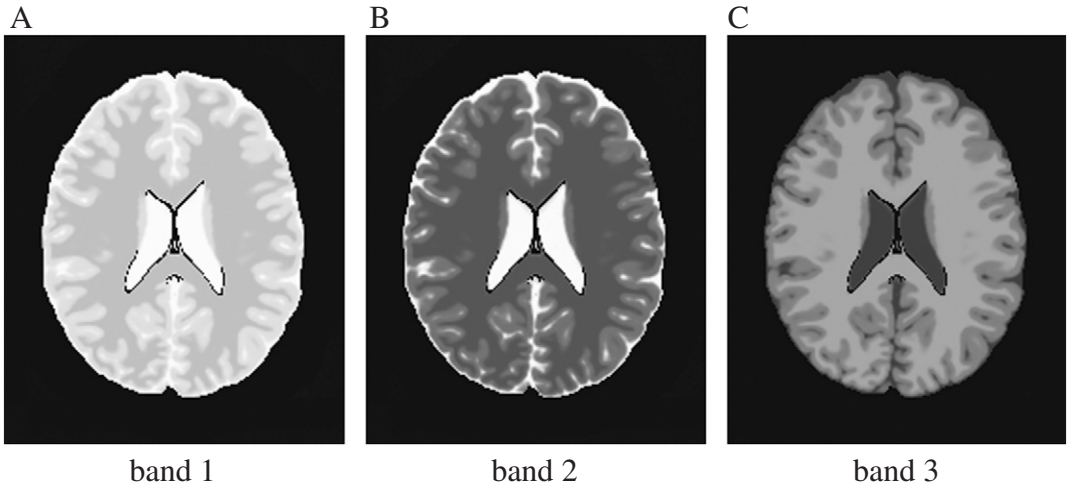

Fig. 6. Three bands of Brainweb MR image, where bands 1, 2 and 3 are PD-weighted, T2-weighted and T1-weighted images, respectively.

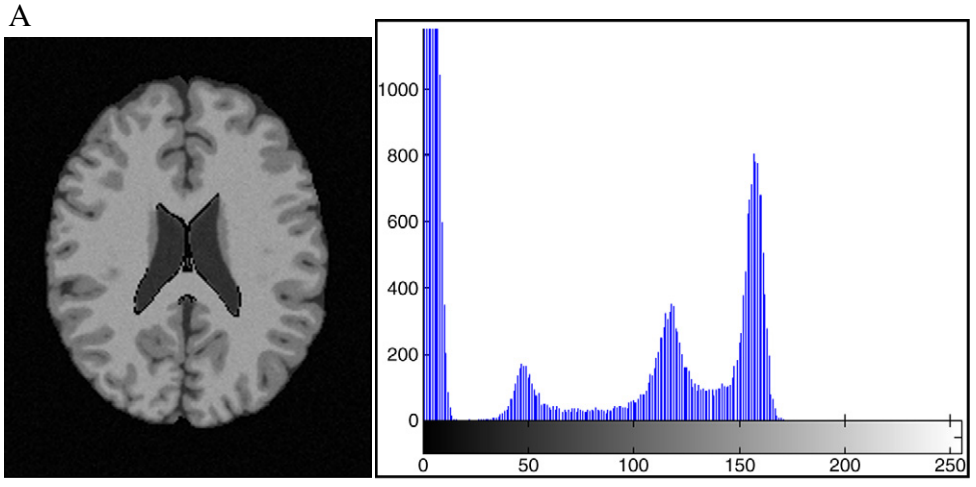

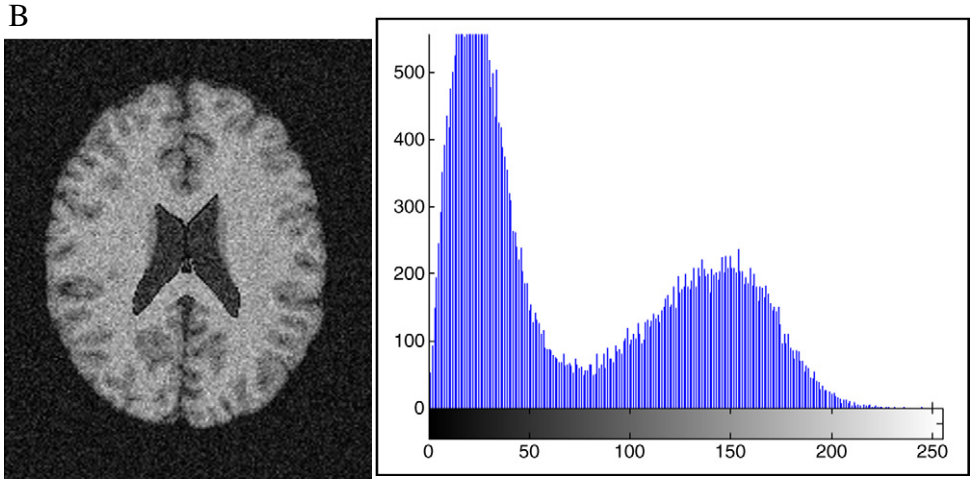

Fig. 7. Added noise phantom images and histograms.

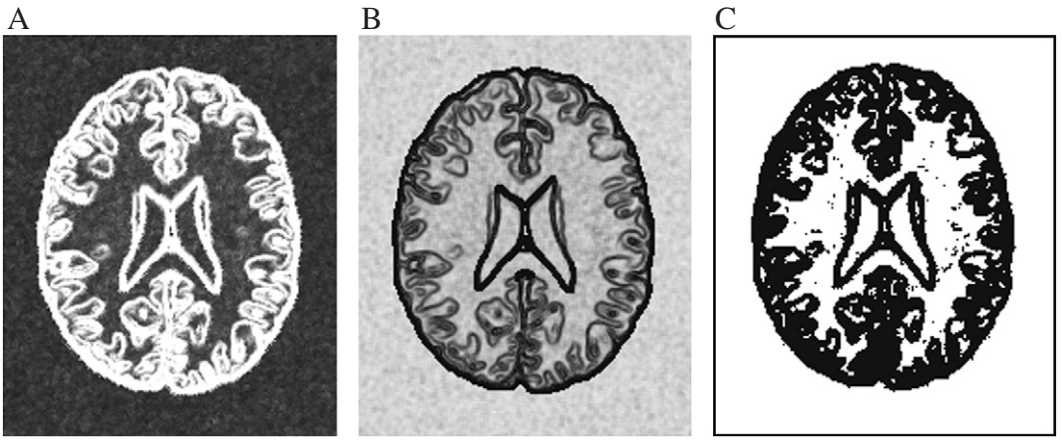

Fig. 8. Some processes of FKSRG in Fig. 6 with Rician noise SNR=20 db. (A) The connected edge *DE*; (B) the fuzzy similarity *S*; (C) the result of initial seeds selection.

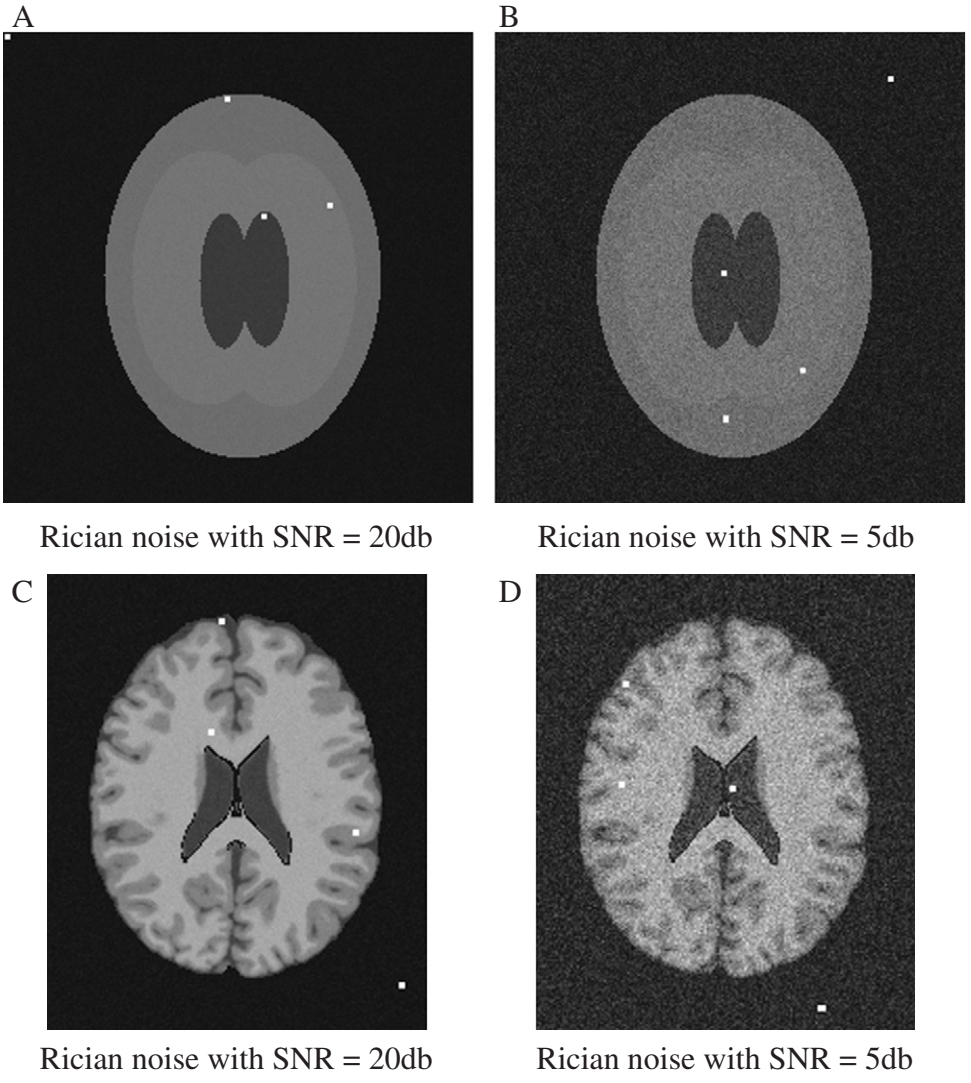

Fig. 9. The targets generated by TGP for added noise phantom images. (The white points are targets.)

However, these processes are not suitable to be applied in MR images because CSF and GM are always represented on edges of MR images. Particularly, most cortical CSF is very thin and is represented by one or two pixels, and these pixels may be assigned to the wrong regions. Therefore, the neighboring seeded regions of $\mathbf{x}^{M}_{x,y}$ in Eq. (8) are modified to all seeded regions. The $\mathbf{x}^{M}_{x,y}$ will be assigned to one of all seeded regions, not one of neighboring seeded regions. After a pixel is labeled to one region and is then removed from M, its unlabeled neighbors are added to M. Thus, the regions' mean $\mathbf{R}_z$, z=1, 2,…, Z are updated. The modified regions growing step proceeds iteratively until M is empty, i.e., all pixels in an image are labeled.

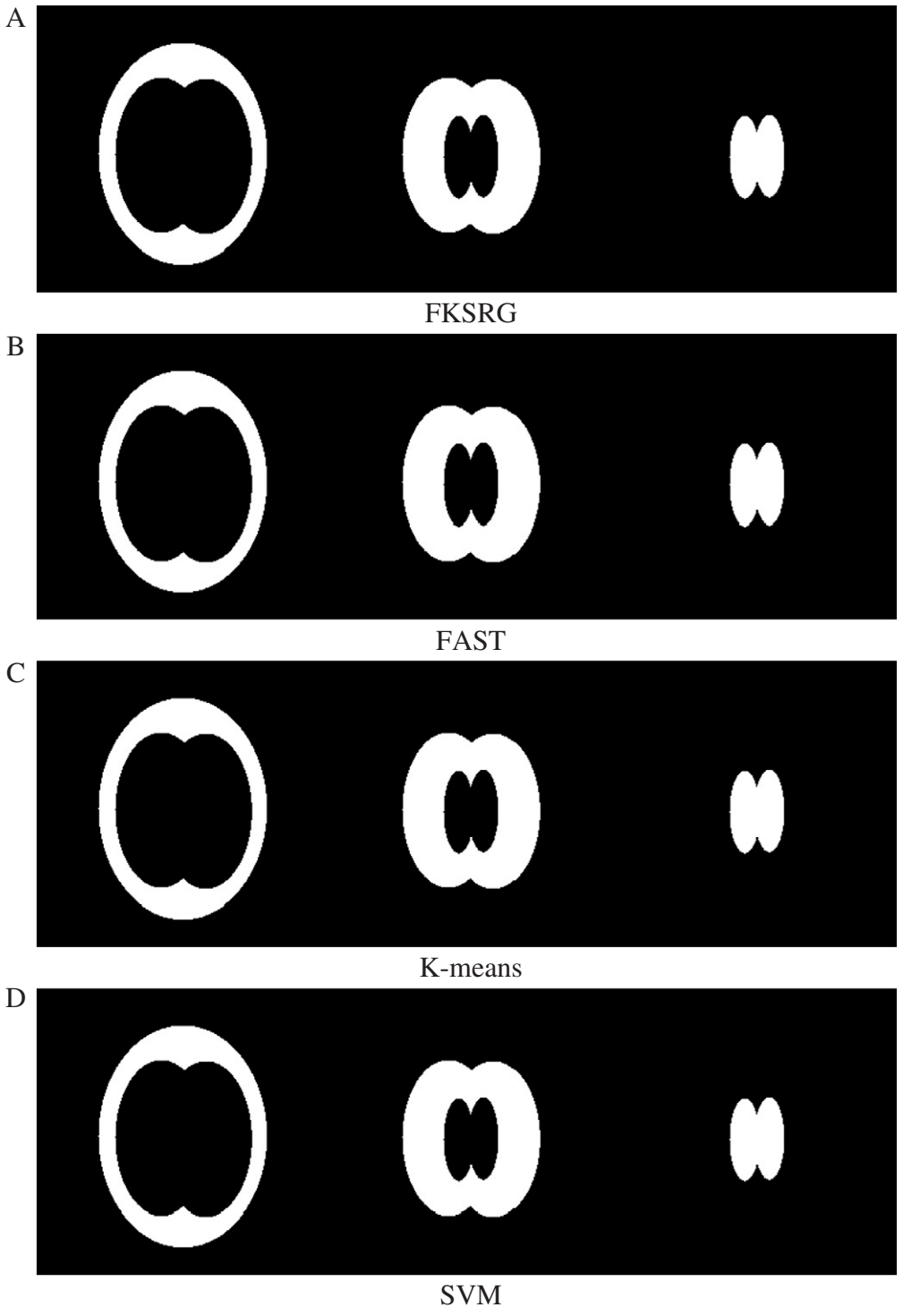

Fig. 10. Classification results by FKSRG, FAST, K-means and SVM for added noise ellipse images with SNR=20 db. From the left to the right of figures are GM, WM and CSF, respectively.

4.3. Regions merging with TGP

In conventional regions merging, the pair of regions with the shortest distance is merged. Thus, the number of segmented regions is unknown. To guarantee that the regions merging process does not over- or undermerge, the TGP is proposed and applied for regions merging. The objective of the TGP is to generate a set of potential target signatures from GM, WM and CSF. The detailed description and algorithm of TGP have been described in Ref. [29] Since TGP generates automatically a set of target pixel vectors' matrices $\mathbf{U}=\{\mathbf{D}^1, \mathbf{D}^2,\ldots, \mathbf{D}^h\}$ and then their vectors' mean

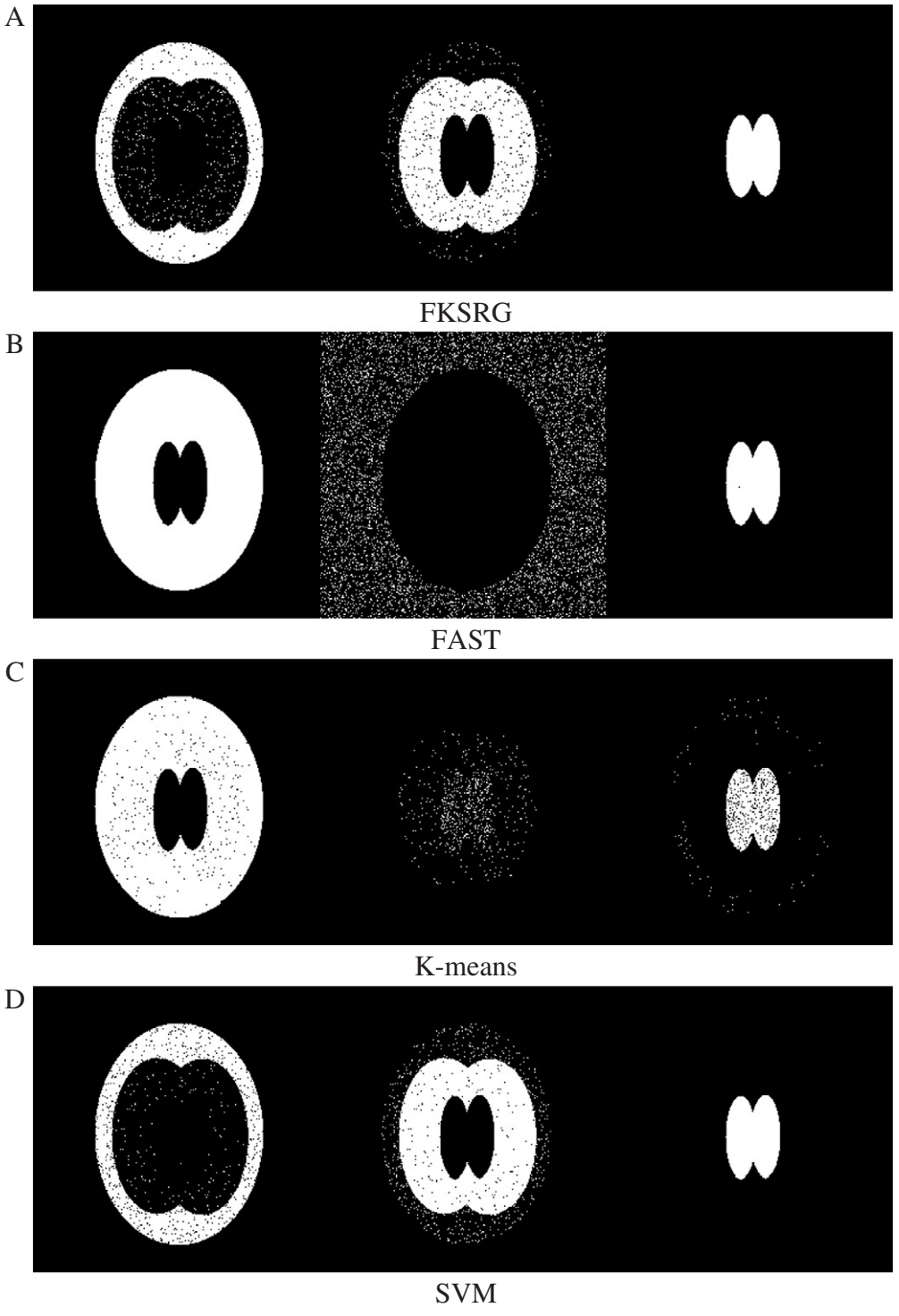

Fig. 11. Classification results by FKSRG, FAST, K-means and SVM for added noise ellipse images with SNR=5 db. From the left to the right of figures are GM, WM and CSF, respectively.

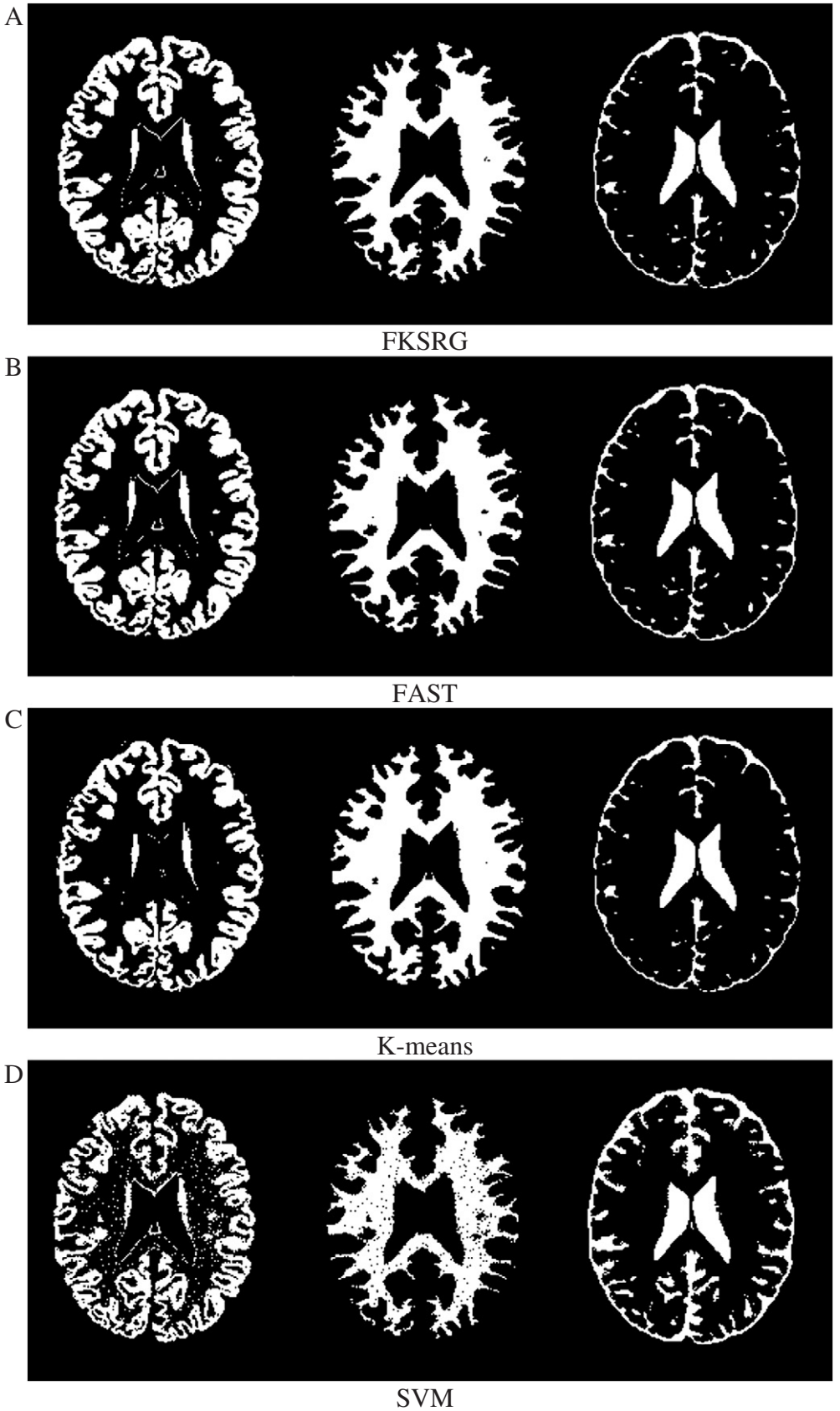

Fig. 12. Classification results by FKSRG, FAST, K-means and SVM for added noise Brainweb images with SNR=20 db. From the left to the right of figures are GM, WM and CSF, respectively.

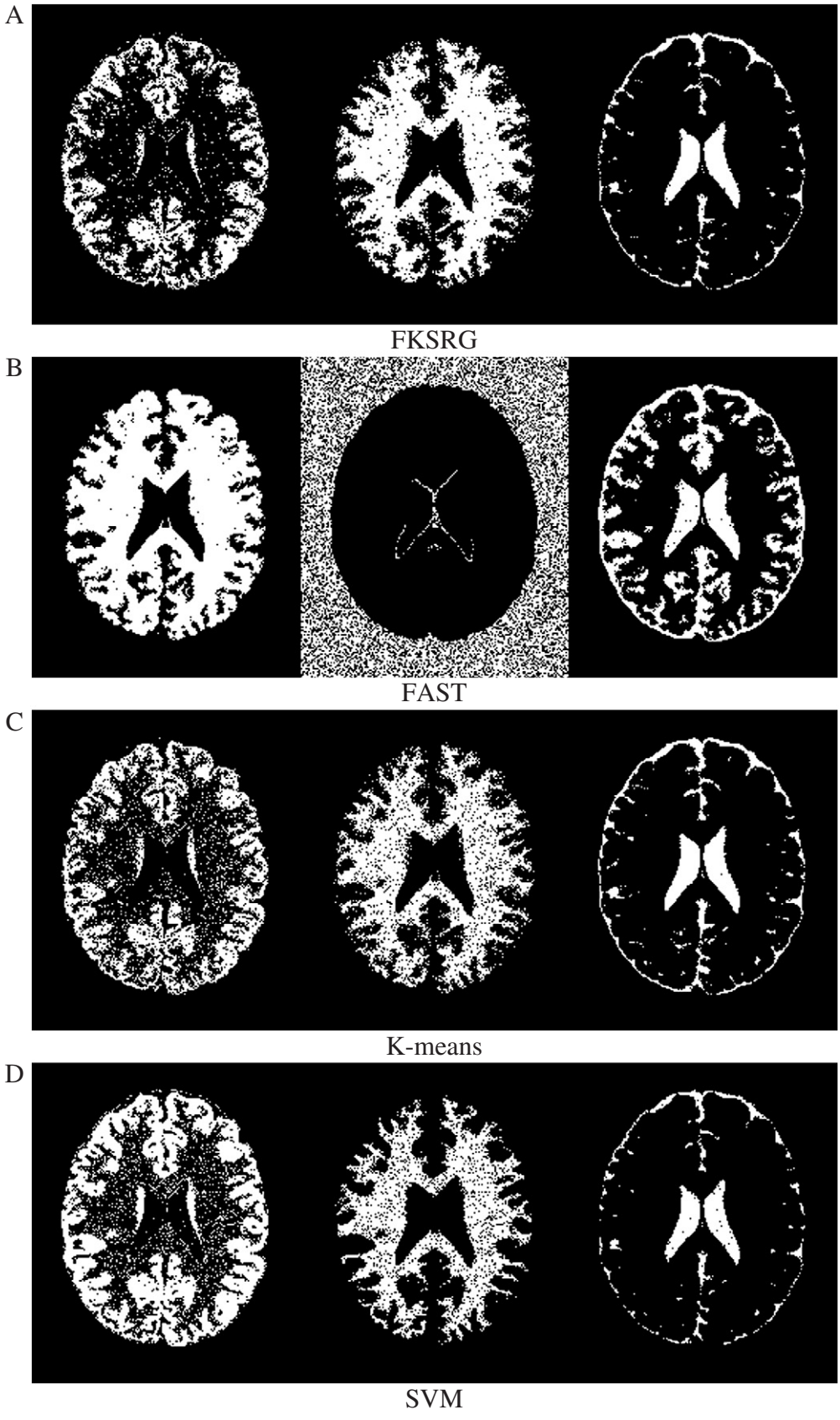

Fig. 13. Classification results by FKSRG, FAST, K-means and SVM for added noise Brainweb images with SNR=5 db. From the left to the right of figures are GM, WM and CSF, respectively.

$\bar{\mathbf{D}}^k$, k=1, 2,..., h are computed, where h is the number of targets. Finally, the labeled region $\mathbf{R}q$, q=1, 2,..., Q, is assigned in the k-th cluster, $k\in\{1, 2,..., h\}$, by Eq. (10):

$$LR_q = \mathrm{Arg}\left(\min_{k\in\{1,2,\ldots,h\}}\left(\left\|\mathbf{R}_q - \overline{\mathbf{D}}^k\right\|\right)\right). \quad (10)$$

where Q is the final number of labeled regions and $LR_q\in\{1, 2,..., h\}$ is the number of clusters in region $\mathbf{R}_q$.

5. Experimental results

An experiment was performed using two image sets, namely, a set of computer-generated phantom images and a set of real MR images. First, the performance of the proposed FKSRG, FAST, K-means and SVM methods was compared using the phantom image set. Notably, the FAST and K-means methods were run with three and four preassigned classes to classify three tissues, WM, GM and CSF, and the background (BKG) of phantom images and real MR images without tumors. SVM was performed with multiclass classification by one-versus-one. The kernel of SVM was polynomial kernel. In order to ensure fairness, the target pixel vectors' matrices $\mathbf{U}=\{\mathbf{D}^1, \mathbf{D}^2,..., \mathbf{D}^h\}$ of TGP were used for training data of SVM. Second, the utility and effectiveness of the FKSRG method for medical diagnosis are evaluated with real multispectral MR images.

5.1. Phantom images experiment

Several computer simulations were performed to compare the performance of the proposed FKSRG method with that of the FAST, K-means and SVM methods. Two image types were utilized — computer-generated ellipse images and simulated brain images downloaded from Brainweb (http://www.bic.mni.mcgill.ca/brainweb). Because MR images are known to follow the Rician distribution, some Rician distributions (noise) with different variances of signal-to-noise ratio (SNR) were added, where the form of signal-to-noise ratio is SNR=20 $\log_{10}$ (signal/noise). Fig. 4 shows the computer-generated ellipse images utilized in simulations. Each image has five bands; each band is 256×256 in size and is made up of overlapping ellipses. These ellipses represent the cerebral GM, WM and CSF (Fig. 5). Band 1 was the PD-weighted simulated image. Bands 2, 3 and 4 were T2-weighted simulated images. Band 5 was the T1-weighted simulated image. Table 1 lists each tissue in its different band, which has a corresponding gray level. Other simulated images are downloaded from Brainweb. Brainweb provides a simulated brain database, which includes a set of realistic MRI data volumes generated by an MRI simulator. The images of the simulated PD-weighted, T2-weighted and T1-weighted with size 181×217×181 in this session were downloaded from Brainweb. Fig. 6 (a–c) shows three bands of a multispectral MR image established by the 95th slice of MRI data in Brainweb database, where bands 1, 2 and 3 are PD-weighted, T2-weighted and T1-weighted images, respectively. Fig. 7 (a–b) illustrates various SNR images and their histograms. Fig. 8 (a–c) shows some processes in FKSRG (Fig. 6) with Rician noise SNR=20 db. Fig. 8 (a and b) shows the connected edge map, *DE*, and fuzzy similarity, *S*, respectively. To represent *DE* and *S* as two images, the fuzzy membership degrees are normalized in the region [0, 255], in which the large fuzzy membership degree leads to high image intensity. Fig. 8 (c) shows the initial seeds denoted as white points. These ellipse images are unrealistic, but demonstrate the use and advantages of the proposed FKSRG method. The performance indices of the FKSRG, FAST and K-means methods were calculated using receiver operating characteristic analysis [5,30].

Table 2
The average classification (detection) rates of FKSRG, FAST, K-means and SVM

	SNR=20 db	SNR=15 db	SNR=10 db	SNR=5 db
(a) Ellipse images				
FKSRG	100%	99.99%	99.97%	98.01%
FAST	100%	99.99%	99.98%	72.48%
K-means	100%	92.90%	92.02%	82.86%
SVM	100%	100%	99.77%	97.94%
(b) Brainweb images				
FKSRG	97.69%	96.37%	95.66%	90.21%
FAST	96.24%	95.38%	84.85%	74.22%
K-means	94.44%	92.17%	88.60%	82.47%
SVM	85.73%	94.43%	91.94%	89.10%

The objects of interest in the MR images were GM, WM and CSF. Let parameters $\mathbf{o}_1$, $\mathbf{o}_2$ and $\mathbf{o}_3$ represent GM, WM and CSF, respectively. Furthermore, $N(\mathbf{o}_i)$, $N_d(\mathbf{o}_i)$, $N_f(\mathbf{o}_i)$ and N_t represent the total number of pixels specified by the i-th object, pixels specified by the i-th object, those actually detected by FKSRG (or FAST or K-means), false-alarm pixels not specified by the i-th object but detected as the i-th object by FKSRG (or FAST or K-means) and pixels of the band image, respectively. The detection rate, $R_d(\mathbf{o}_i)$, false

Table 3
The average false alarm rates of FKSRG, FAST, K-means and SVM

	SNR=20 db	SNR=15 db	SNR=10 db	SNR=5 db
(a) Ellipse images				
FKSRG	0%	0%	0.01%	0.52%
FAST	0%	0%	0.01%	12.64%
K-means	0%	1.35%	1.39%	8.02%
SVM	0%	0%	0.06%	0.58%
(b) Brainweb images				
FKSRG	1.09%	1.13%	1.30%	4.13%
FAST	1.43%	1.49%	8.25%	21.15%
K-means	1.81%	1.88%	4.56%	8.38%
SVM	3.26%	1.87%	1.65%	3.23%

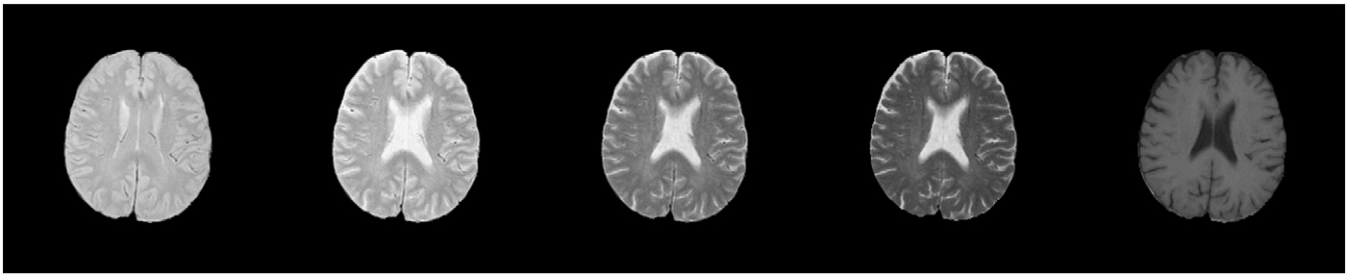

Fig. 14. Five bands of the multispectral real MR image. Band 1 is the PD-weighted spectral image obtained from the pulse sequence TR/TE=2500 ms/25 ms. Bands 2, 3 and 4 are T2-weighted spectral images acquired from the pulse sequences TR/TE=2500 ms/50 ms, TR/TE=2500 ms/75 ms and TR/TE=2500 ms/100 ms, respectively. Band 5 is the T1-weighted spectral image acquired from the pulse sequence TR/TE=500 ms/11.9 ms.

rate, $R_f(\mathbf{o}_i)$, mean detection rate, $\overline{R}_d$, and mean false-alarm rate, $\overline{R}_f$, are defined as follows:

$$R_d(\mathbf{o}_i) = \frac{N_d(\mathbf{o}_i)}{N(\mathbf{o}_i)}, \tag{11}$$

$$R_f(\mathbf{o}_i) = \frac{N_f(\mathbf{o}_i)}{N_t - N(\mathbf{o}_i)}, \tag{12}$$

$$\overline{R}_d = \sum_{i=1}^{3} R_d(\mathbf{o}_i) P(\mathbf{o}_i) \tag{13}$$

and

$$\overline{R}_f = \sum_{i=1}^{3} R_f(\mathbf{o}_i) P(\mathbf{o}_i), \tag{14}$$

respectively, where $P(\mathbf{o}_i) = N(\mathbf{o}_i) / \sum_{i=1}^{3} N(\mathbf{o}_i)$. The initial class centers for the K-means and FAST methods and the initial target for the TGP were generated randomly. To compare the performance of the FKSRG, FAST, K-means and SVM methods equitably, each method was applied 100 times. The thresholds for initial seeds selection were set at 0.6, 0.7, 0.7 and 0.7, corresponding to images with SNR=20 db, SNR=15 db, SNR=10 db and SNR=5 db, respectively. In our experimental experiences, we suggest to set threshold in the region [0.5, 0.8]. If the threshold is set too small, some seeds would be mixed together. If the threshold is set too large, the algorithm would cost more time in region growing. In the TGP, h=4 indicates that four targets are generated. To avoid more images being shown in this study, we only show the result images of SNR=20 and 5 db. Fig. 9 (a–b) shows the targets generated by the TGP. Figs. 10 and 11 show experimental results of running FKSRG, FAST, K-means and SVM to the ellipse images with SNR=20 db and 5 db, respectively. Figs. 12 and 13 show experimental results from applying the FKSRG, FAST, K-means and SVM methods, respectively, to Brainweb images with SNR=20 db and 5 db, respectively. The FAST and K-means methods produced false classifications for images with SNR=5 db (Figs. 11 and 13). Figs. 11 (b–c) and 13 (b–c) show false classification results produced by the FAST and K-means method. In this experiment, the K-means approach produced 24 and 20 successful classifications of ellipse images and Brainweb images with SNR=5 db, respectively. The FKSRG and SVM method produced 100 successful classifications for the same images. Notably, the FAST scheme had no successful classifications. Tables 2 and 3 present the average classification rates (detection rates) and false-alarm rates produced by the FKSRG, FAST, K-means and SVM schemes with SNR=20 db, 15 db, 10 db and 5 db with 100 runs, respectively. These analytical results suggest that the performance of the proposed FKSRG scheme is much better than that of the other approaches for images with SNR=20 db, 15 db, 10 db and 5 db. Although SVM also has high classification rates, SVM performed a poor classification rate for Brainweb images with SNR=20 db. Overall, the FKSRG scheme has the best segmentation capability for multispectral MR images and is robust to noise.

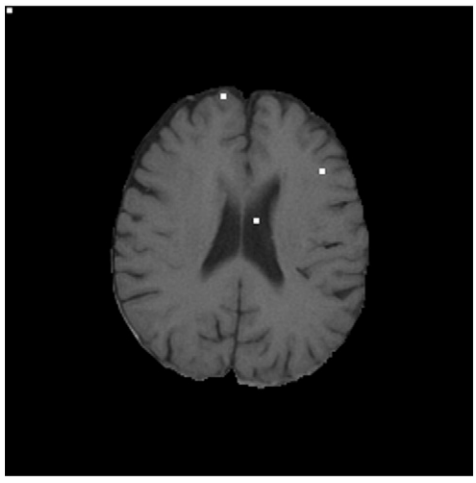

Fig. 15. The targets generated by TGP for the image in Fig. 13. (The white points are targets.)

5.2. Real MR image experiments

5.2.1. Real MR Images without tumor

Real MR images were acquired from 10 people with normal physiologies. Fig. 14 shows one example image. The resolution and size of each band were 8-bit gray level and 256×256 pixels, respectively. Band 1 was the PD-weighted spectral image obtained from the pulse sequence TR/TE=2500 ms/25 ms. Bands 2, 3 and 4 were T2-weighted spectral images acquired from the pulse sequences TR/TE=2500 ms/50 ms, TR/TE=2500 ms/75 ms and TR/TE=2500 ms/100 ms, respectively. Band 5 was the T1-weighted spectral image acquired from the pulse sequence TR/TE=500 ms/11.9 ms. An MR image slice was

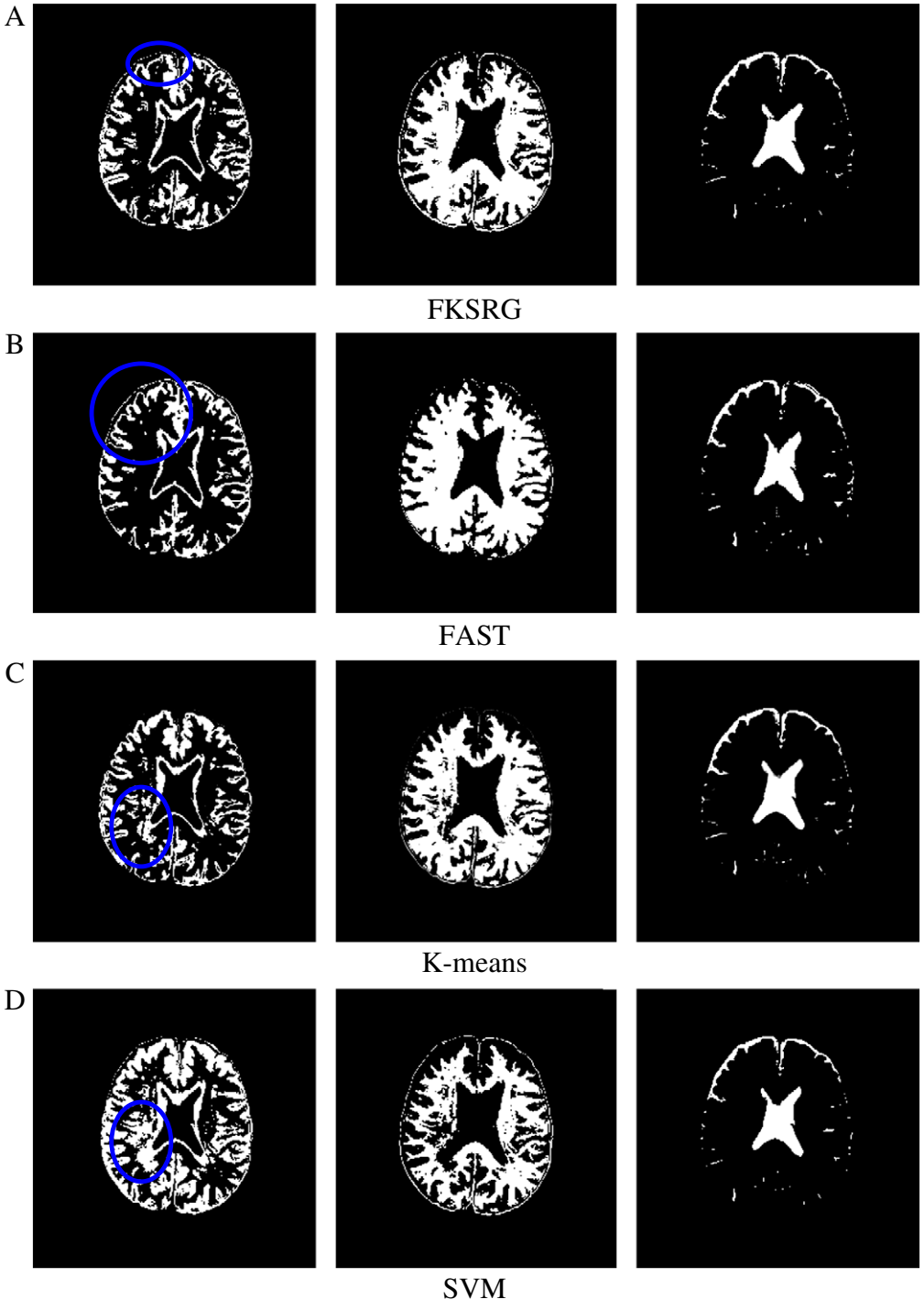

Fig. 16. Classification results by FKSRG, FAST, K-means and SVM for the image in Fig. 14. From the left to the right of figures are GM, WM and CSF, respectively. The parts enclosed by blue circles indicate incorrectly classified GM and WM.

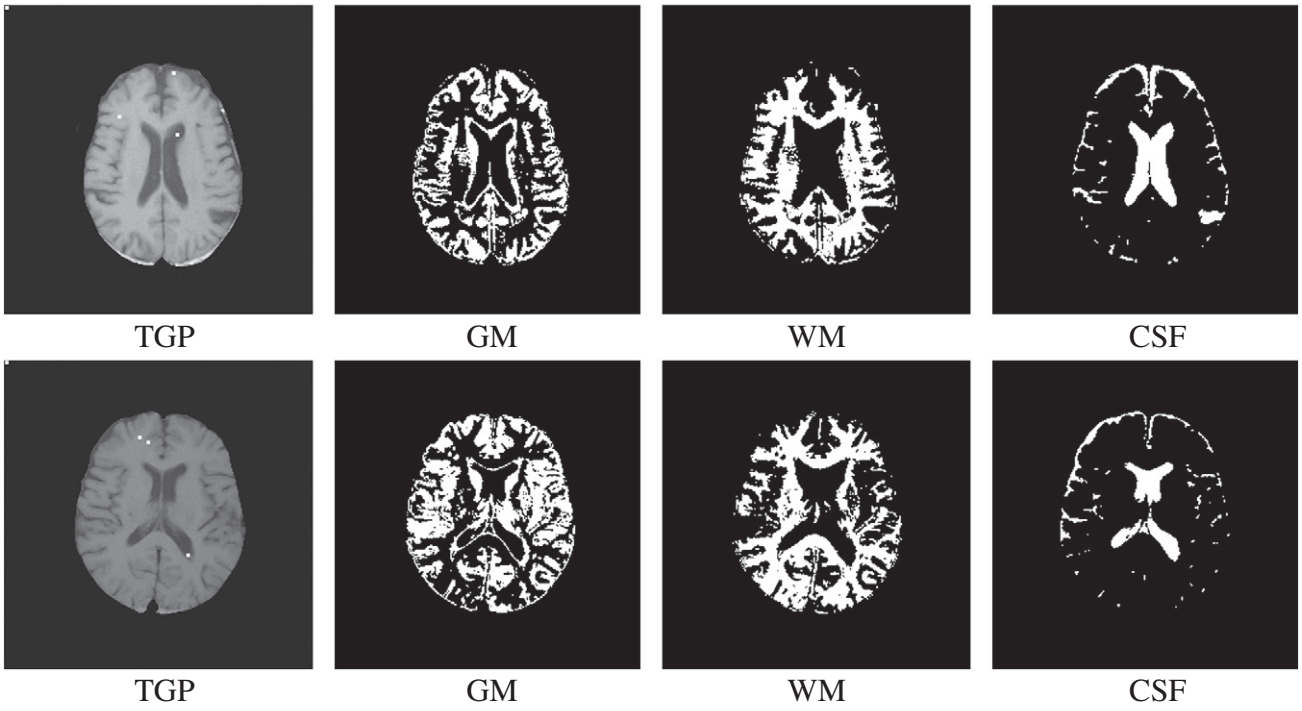

Fig. 17. The TGP and classification results of other two subjects by FKSRG.

6 mm thick, and its axial section was taken by a GE MR 1.5-T Scanner. Before obtaining MR images for the experiment, the static magnetic field, radio frequency and gradient of the scanner were adjusted to achieve the desired accuracy. All experiments were performed under supervision by experienced neuron radiologists. The images were preprocessed before experiments, that is, tissues near the brain (bone, fat and skin) were removed semiautomatically using the interactive thresholding and masking method in Ref. [31]. The threshold of initial seeds selection and h of the TGP were set at 0.7 and 4, respectively. Fig. 15 shows the targets generated by the TGP. Fig. 16 (a–d) shows classification results obtained by the FKSRG, FAST, K-means and SVM methods, respectively. The parts enclosed by blue circles indicate incorrectly classified GM and WM. Fig. 17 shows the TGP and classification of other subjects by the proposed FKSRG approach. Overall, the FKSRG scheme had the fewest incorrect classifications. Thus, the FKSRG approach produced better results than did the FAST, K-means and SVM methods. It should be stressed that all the experimental results presented herein were verified by experienced radiologists.

5.2.2. Real MR images with tumor

Another set of multispectral MR brain image was then considered. This set comprised several MR images (Fig. 18) acquired from a patient with a brain tumor. The images had four bands with 8-bit gray-level resolution and were sized 256×256 pixels. The T1-weighted and T2-weighted images were obtained for bands 1 and 2, respectively, while the PD-weighted and Gadopentetic acid-Diethylene-TriaminePentAcetic acid images were obtained for bands 3

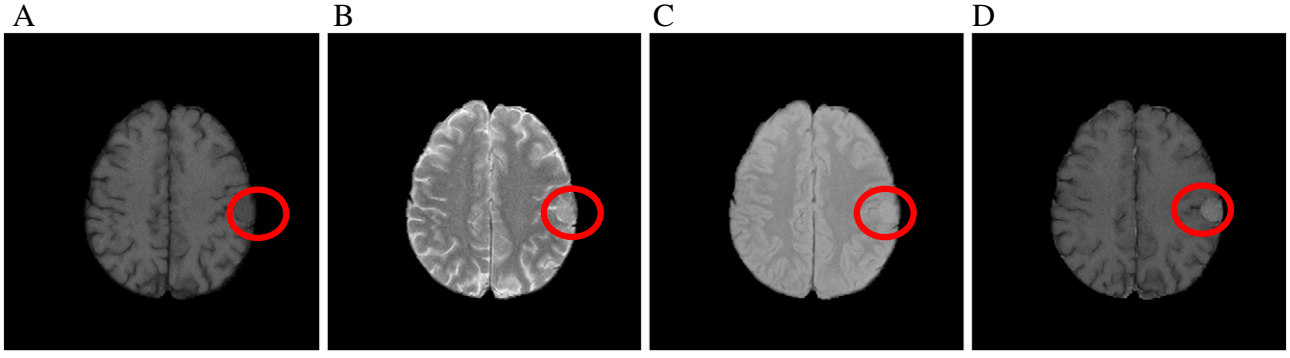

Fig. 18. The MR images of the brain with tumor. (The tumor is enclosed by a red circle.)

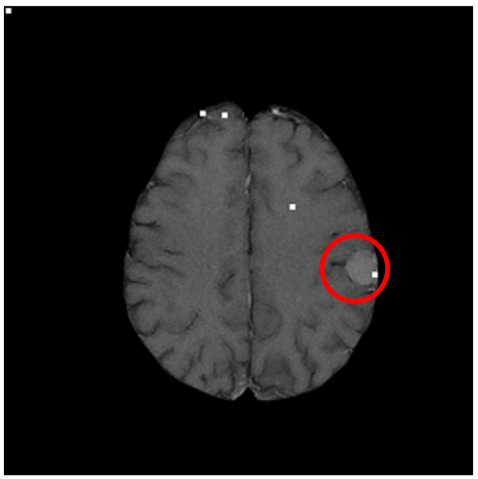

Fig. 19. The targets generated by TGP for the image in Fig. 18. (The white points are targets.)

and 4, respectively. The thickness of each MR image slice was 2 mm, and its axial section was taken from Signa 1.5-T SYS#GEMSOW. All experiments were supervised by a neuron radiologist, and all spectra were extracted directly from MR images and verified by experienced radiologists. In this experiment, the FAST, K-means and SVM methods were run with four and five preassigned classes to classify three tissues, the tumor and BKG. The threshold of initial seeds selection and h of the TGP were set to 0.7 and 5, respectively. Fig. 19 displays the targets generated by the TGP. Fig. 20 (a–d) shows tumor segmentation results by the FKSRG, FAST, K-means and SVM methods for the four images (Fig. 18). In Fig. 20 (a–d), the tumor is enclosed by a red circle. The proposed FKSRG approach and SVM segmented the tumor more clearly than did the FAST and K-means methods. Interestingly, SVM performed the almost perfect segmentation result. All the experimental results presented herein were verified by experienced radiologists.

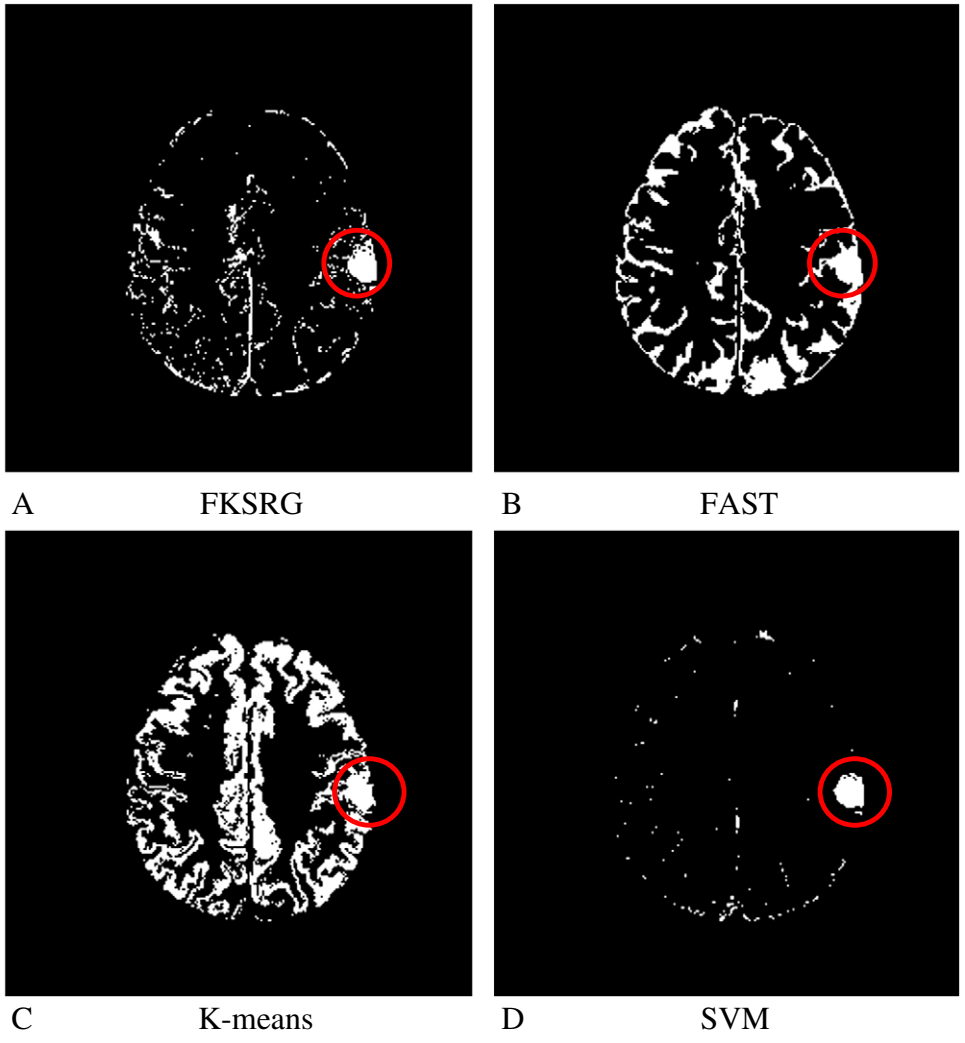

Fig. 20. The segmentation results of tumor by FKSRG, FAST, K-means and SVM for the image in Fig. 18. The segmented tumor is enclosed by a red circle.

6. Conclusions

This work presented a novel SRG-based image segmentation method for multispectral MR images called FKSRG. Fuzzy edge detection in this work is modified to detect connected edges. The initial seeds without a detailed and complex BKG are selected automatically by combining fuzzy edge and fuzzy similarity. Each initial seed region grows gradually by checking the fuzzy distance between a pixel and all seeded regions until the entire image is segmented. The conventional regions growing methods is also modified to ensure that a pixel on an edge is processed later than other pixels. To guarantee that the proposed method does not over- or undersegment, the proposed TGP is applied to regions merging. The performance of the FKSRG, FAST and K-means methods was measured experimentally using two image sets, namely, computer-generated phantom images and real MRI images. Experimental results demonstrate that FKSRG is markedly better and effective at segmentation for multispectral MR images than the FAST and K-means methods, even when a processed image is disturbed by some noise.

Acknowledgment

The authors would like to thank Dr. Sheng-Yih Sun of the Department of Radiology in Tao-Yuan General Hospital for his suggestions.

References

[1] Wright GA. Magnetic resonance imaging. IEEE Signal Process Mag 1997;14:56–66.
[2] Sebastiani G, Barone P. Mathematical principles of basic magnetic-resonance-imaging in medicine. Signal Process 1991;25:227–50.
[3] Wang CM, Chen CCC, Yang SC, Chung PC, Chung YN, Yang CW, Chang CI. Unsupervised orthogonal subspace projection approach to magnetic resonance image classification. Opt Eng 2002;41:1546–57.
[4] Wang CM, Yang SC, Chung PC, Chang CI, Lo CS, Chen CC, Yang CW, Wen CH. Orthogonal subspace projection-based approaches to classification of MR image sequences. Comput Med Imag Grap 2001;25:465–76.
[5] Wang CM, Chen CCC, Chung YN, Yang SC, Chung PC, Yang CW, Chang CI. Detection of spectral signatures in multispectral MR images for classification. IEEE Trans Med Imaging 2003;22:50–61.
[6] Wang CM, Lin GC, Lin CY, Chen RM. An unsupervised Kalman filter-based linear mixing approach to MRI classification, 2004 IEEE Asia-Pacific Conference on Circuits and Systems. Tainan (Taiwan ROC) 2004:1105–8.
[7] Reddick WE, Glass JO, Cook EN, Elkin TD, Deaton RJ. Automated segmentation and classification of multispectral magnetic resonance images of brain using artificial neural networks. IEEE Trans Med Imaging 1997;16:911–8.
[8] Alirezaie J, Jernigan ME, Nahmias C. Automatic segmentation of cerebral MR images using artificial neural networks. IEEE Trans Nucl Sci 1998;45:2174–82.
[9] Lin JS, Chen RM, Huang YM. Medical image segmentation using mean field annealing network. IEEE International Conference on Image Processing, Washingtom, D.C. (USA); 1997. p. 855–8.
[10] Lin JS, Cheng KS, Mao CW. Multispectral magnetic resonance images segmentation using fuzzy Hopfield neural network. Int J Biomed Comput 1996;42:205–14.
[11] Ahmed MN, Yamany SM, Mohamed N, Farag AA, Moriarty T. A modified fuzzy C-means algorithm for bias field estimation and segmentation of MRI data. IEEE Trans Med Imaging 2002;21:193–9.
[12] Chuang KH, Chiu MJ, Lin CC, Chen JH. Model-free functional MRI analysis using Kohonen clustering neural network and fuzzy c-means. IEEE Trans Med Imaging 1999;18:1117–28.
[13] Zhao Y, Li M. A modified fuzzy c-means algorithm for segmentation of MRI. Fifth International Conference on Computational Intelligence and Multimedia Applications, Xi'an (China); 2003. p. 391–5.
[14] Ahmed MN, Yamany SM, Farag AA, Moriarty T. Bias field estimation and adaptive segmentation of MRI data using a modified fuzzy C-means algorithm. IEEE Computer Society Conference on Computer Vision and Pattern Recognition, Fort Collins, CO.(USA); 1999. p. 23–5.
[15] Mohamed NA, Ahmed MN, Farag AA. Modified fuzzy c-mean in medical image segmentation. IEEE International Conference on Acoustics, Speech, and Signal Processing, Phoenix, Arizona(USA); 1999. p. 3429–32.
[16] Clark MC, Hall LO, Goldgof DB, Velthuizen R, Murtagh FR, Silbiger MS. Automatic tumor segmentation using knowledge-based techniques. IEEE Trans Med Imaging 1998;17:187–201.
[17] Zhang YY, Brady M, Smith S. Segmentation of brain MR images through a hidden Markov random field model and the expectation-maximization algorithm. IEEE Trans Med Imaging 2001;20:45–57.
[18] Wang CM, Kuo CT, Lin CY, Chang GH. Application of artificial immune system approach in MRI classification. EURASIP J Adv Signal Process, Volume 2008, doi:10.1155/2008/547684.
[19] He RJ, Sajja BR, Datta S, Narayana PA. Volume and shape in feature space on adaptive FCM in MRI segmentation. Ann Biomed Eng 2008;36:1580–93.
[20] Bricq S, Collet C, Armspach JP. Unifying framework for multimodal brain MRI segmentation based on hidden Markov chains. Med Image Anal 2008;12:639–52.
[21] Adams R, Bischof L. Seeded region growing. IEEE Trans Pattern Anal Mach Intell 1994;16:641–7.
[22] Fan JP, Yau DKY, Elmagarmid AK, Aref WG. Automatic image segmentation by integrating color-edge extraction and seeded region growing. IEEE Trans Image Process 2001;10:1454–66.
[23] Fan HP, Zeng GH, Body M, Hacid MS. Seeded region growing: an extensive and comparative study. Pattern Recognit Lett 2005;26:1139–56.
[24] Shih FY, Cheng SX. Automatic seeded region growing for color image segmentation. Image Vis Comput 2005;23:877–86.
[25] Deng YN, Manjunath BS. Unsupervised segmentation of color-texture regions in images and video. IEEE Trans Pattern Anal Mach Intell 2001;23:800–10.
[26] Kang CC, Wang WJ. A novel edge detection method based on the maximizing objective function. Pattern Recognit 2007;40:609–18.
[27] FMRIB's automated segmentation tool — http://www.fmrib.ox.ac.uk/analysis/research/fast/.
[28] Cortes C, Vapnik V. Support vector networks. Mach Learn 1995;20:273–97.
[29] Lin GC, Wang WJ, Wang CM, Sun SY. Automated classification of multi-spectral MR images using linear discriminant analysis. Comput Med Imag Grap 2010;34:251–68.
[30] van Erkel AR, Pattynama PMT. Receiver operating characteristic (ROC) analysis: basic principles and applications in radiology. Eur J Radiol 1998;27:88–94.
[31] Suzuki H, Toriwaki J. Automatic segmentation of head MR images by knowledge guided thresholding. Comput Med Imag Grap 1991;15:233–40.